Science Bulletin 68 (2023) 730–739

Contents lists available at ScienceDirect

Science Bulletin

journal homepage: www.elsevier.com/locate/scib

Article

Predicting residual friction angle of lunar regolith based on Chang'e-5 lunar samples

Jiayan Nie [a,b], Yifei Cui [a,*], Kostas Senetakis [c], Dan Guo [d], Yu Wang [e], Guodong Wang [a], Peng Feng [f], Huaiyu He [g], Xuhang Zhang [g], Xiaoping Zhang [h], Cunhui Li [i], Hu Zheng [j], Wei Hu [k], Fujun Niu [l], Quanxing Liu [m], Anyuan Li [n]

[a] State Key Laboratory of Hydroscience and Engineering, Tsinghua University, Beijing 100084, China
[b] School of Civil Engineering, Wuhan University, Wuhan 430072, China
[c] Department of Architecture and Civil Engineering, City University of Hong Kong, Hong Kong 999077, China
[d] State Key Laboratory of Tribology, Tsinghua University, Beijing 100084, China
[e] Key Laboratory of Mountain Hazards and Surface Process, Institute of Mountain Hazards and Environment, Chinese Academy of Sciences, Chengdu 610041, China
[f] Department of Civil Engineering, Tsinghua University, Beijing 100084, China
[g] State Key Laboratory of Lithospheric Evolution, Institute of Geology and Geophysics, Chinese Academy of Sciences, Beijing 100029, China
[h] State Key Laboratory of Lunar and Planetary Sciences, Macau University of Science and Technology, Macau 999078, China
[i] Science and Technology on Vacuum Technology and Physics Laboratory, Lanzhou Institute of Physics, Lanzhou 730000, China
[j] Department of Geotechnical Engineering, College of Civil Engineering, Tongji University, Shanghai 200092, China
[k] State Key Laboratory of Geohazard Prevention and Geoenvironment Protection, Chengdu University of Technology, Chengdu 610059, China
[l] South China Institute of Geotechnical Engineering, South China University of Technology, Guangzhou 510641, China
[m] School of Mathematical Sciences, Shanghai Jiao Tong University, Shanghai 200240, China
[n] Key Laboratory of Rock Mechanics and Geohazards of Zhejiang Province, Shaoxing University, Shaoxing 312000, China

ARTICLE INFO

Article history:
Received 5 September 2022
Received in revised form 4 March 2023
Accepted 6 March 2023
Available online 13 March 2023

Keywords:
Chang'e-5 lunar samples
Geometry
Mechanics
Tribology
Residual friction angle
Cross-scale prediction

ABSTRACT

With the rapid development of human lunar exploration projects, the lunar base establishment and resource utilization are on the way, and hence it is urgent and significant to reasonably predict engineering properties of the lunar regolith, which remains to be unclear due to limited lunar samples currently accessible for geotechnical tests. In this contribution, we aim to address this outstanding challenge from the perspective of granular material mechanics. To this end, the 3D multi-aspect geometrical characteristics and mechanical properties of Chang'e-5 lunar samples are for the first time evaluated with a series of non-destructive microscopic tests. Based on the measured particle surface roughness and Young's modulus, the interparticle friction coefficients of lunar regolith particles are well predicted through an experimental fitting approach using previously published data on terrestrial geomaterials or engineering materials. Then the residual friction angle of the lunar regolith under low confining pressure is predicted as 53° to 56° according to the particle overall regularity and interparticle friction coefficients of Chang'e-5 lunar samples. The presented results provide a novel cross-scale method to predict engineering properties of the lunar regolith from particle scale information to serve for the future lunar surface engineering construction.

1. Introduction

The Moon, being the only natural satellite of our beautiful planet, has always attracted the human attention, and exploring the Moon is the first step of humans to explore the vast space. During the US Apollo and Soviet Luna periods (1960s and 1970s), a large amount of lunar data had been returned back to the Earth, and important studies had been performed to understand the physical, chemical and mechanical properties of the lunar regolith [1–4]. Recently, with the immense success of the China's Lunar Exploration Program (Chang'e project) and the start-up of the American Artemis Program [5,6], a new round of "return to the Moon" boom has risen, and space agencies all around the world have been already working on the future lunar manned expeditions and base establishment in order to utilize the lunar resources and further explore other planets, taking the Moon as the transferring station. The successful implementation of these rather challenging projects relies heavily on the exact evaluation of the *in-situ* performance of the lunar regolith under external loads, which is far from being understood thoroughly from previous limited lunar exploration missions due to the heterogeneity of the lunar regolith at different sampling sites.

* Corresponding author.
E-mail address: yifeicui@mail.tsinghua.edu.cn (Y. Cui).

https://doi.org/10.1016/j.scib.2023.03.019

In December 1, 2020 (Beijing time), China's Chang'e-5 probe landed on a young and flat mare area in the Northern Oceanus Procellarum of the Moon [7], and successfully returned to the Earth with 1731 g lunar samples after completing drilling, shoveling, packing of lunar samples and scientific exploration on the lunar surface. These brand-new lunar samples had further improved our understanding on the formation and evolution of the Earth-Moon system, the chemical evolution history of the lunar surface and also the basic physical properties like particle size, shape, and mineralogical compositions of the lunar regolith [8–13]. Although most current studies on Chang'e-5 lunar samples have been carried out for purely scientific objectives, ongoing lunar surface engineering construction will also require engineering data with regards to mechanical properties of the lunar regolith, which has not received enough attention yet for current lunar sample studies.

The lunar regolith is mainly formed by the degeneration of the bed rock due to the everlasting impact of micrometeorites/meteorites and constant radiation of the solar wind and cosmic rays ever since the formation of the Moon [4]. Because of the unique lunar surface environment (e.g., ultra-high vacuum and extreme temperature), the lunar regolith can be actually considered as a solid cohesive granular material, and primarily consists of crystalline rocks, mineral fragments, and secondary particles like breccias, agglutinates, and glass grains, whose sizes range from a few microns to a few millimeters [4,11,13]. Different types of lunar regolith particles may exhibit different geometrical and mechanical properties [4,13,14]. For instance, the agglutinates generally present branched morphologies with intraparticle voids, giving them a highly vesicular texture, while glass grains can be almost spherical and attached with the agglomeration of other lunar regolith grains [4]. Moreover, the lunar regolith covering the Moon is naturally heterogeneous, which means that the weight percentages of different types of lunar regolith particles are distinct at different sampling sites [15]. The complex particle property characteristics have made engineering properties of the lunar regolith rather complicated and spatially varying, which needs to be scientifically explored based on limited lunar samples. From the perspective of granular material mechanics, the macromechanical behavior of the lunar regolith under external loads depends predominantly on the packing patterns and interactions of different types of constituent particles, which are further correlated with the particle basic properties (e.g., particle size, grading, shape, mineralogy) [16–21]. These particle properties comprise a solid basis for the development of advanced constitutive modeling of geomaterials with broad implications in geophysical researches [22–25], and make it possible to predict engineering properties of the lunar regolith from the particle scale information.

As a cross-scale study on engineering properties of the lunar regolith, we firstly conduct a series of non-destructive microscopic tests on Chang'e-5 lunar samples to acquire their geometrical, tribological, and mechanical properties. Based on the particle basic properties, the residual friction angle of the lunar regolith under low confining pressure, a key indicator for the shear resistance strength of the soil at the critical state, is reasonably predicted. Besides, different effects of surface processes of the Earth and Moon on 3D multi-aspect shape characteristics of terrestrial and lunar soils have been discussed.

2. Materials and methods

2.1. Chang'e-5 lunar samples

One polished section sample of lunar breccia clast (sample ID: CE5C0800YJYX001GP, named BYX001GP for short, Fig. 1a) and two natural lunar basalt clasts (sample IDs: CE5Z0906YJYX005 and CE5Z0709YJYX002, named BYX005 and BYX002, respectively for short, Fig. 1b, c) returned by China's Chang'e-5 mission were used to conduct non-destructive microscopic tests to acquire their geometrical and mechanical properties. The BYX001GP is a scooped sample while the BYX005 and BYX002 are drilled samples. According to the lunar sample naming rules of Chang'e-5 ground application system and previous analysis on Chang'e-5 lunar core drilling process [26], both drilled samples are speculated to be beneath the lunar surface of 0–40 cm. The particle equivalent size of BYX002 (i.e., ~2040 μm) is larger than that of BYX005 (i.e., ~1695 μm). In order to quantify the overall shape characteristic of lunar regolith particles, 222 extra lunar regolith particles covering different types of mineral fragments, basalt and breccia clasts, agglutinates, and glass grains were randomly selected from the scooped bulk sample (sample ID: CE5C0600YJFM00306) to acquire their 3D multi-aspect particle morphology indices, and their equivalent sizes range from ~102 to ~2704 μm.

2.2. Microscopic tests

The X-ray μCT scanning and 3D white light interferometry techniques were adopted to quantify 3D multi-aspect shape indices (i.e., global form, local roundness, and surface roughness in Fig. S1 (online), reference to [27,28]) of lunar regolith particles aided with a series of image processing methods. Among which, the HeliScan μCT scanning apparatus (Fig. 1d) was employed to analyze 3D particle shape features at the former two large scales for a total of 224 natural lunar regolith particles, while the ZYGO NexView 3D white light interferometry apparatus (Fig. 1g) was used to determine the particle surface roughness. For 3D white light interferometry tests, three different sized fields of view (i.e., 20 μm × 20 μm, 40 μm × 40 μm, and 84 μm × 84 μm) were chosen to acquire the corresponding 3D flattened surface roughness profiles (Fig. 1h, i) of BYX005 and BYX002 and further discuss its possible effect on the determined particle surface roughness. For each sized field of view, 15–60 local surface areas were randomly measured to acquire their average value as the representative particle surface roughness.

Nanoindentation tests were conducted to determine the mechanical properties (e.g., Young's modulus and hardness) of lunar regolith particles. Among which, the Hysitron TI 980 TriboIndenter (Bruker) nanoindentation apparatus (Fig. 1j) was used for the polished section sample (i.e., BYX001GP) while the Bruker (Icon) atomic force microscopy (AFM) (Fig. 1m) was employed for the rugged and rough lunar samples (i.e., BYX005 and BYX002). During nanoindentation tests for BYX001GP, four representative measurement areas (MAs) (i.e., MA1–MA4 in Fig. 1k) corresponding to different mineral phases or areas were analyzed. For each MA, six different indented spots were randomly measured to probe into the heterogeneity of lunar regolith materials under three different combinations of maximum applied force F_{max} and creep time t_c (i.e., F_{max} = 10 mN and t_c = 5 s, F_{max} = 10 mN and t_c = 20 s, F_{max} = 50 mN and t_c = 5 s) (Fig. 1l). For nanoindentation tests on BYX005 and BYX002 by AFM, at least 30 different indented spots were chosen randomly to acquire their corresponding material Young's modulus under two different maximum applied forces (i.e., F_{max} = 7.5 and 15 μN) (Fig. 1o). The specific experimental implementation details and determination of relevant physical quantities can be referenced to the Supplementary materials (online).

3. Results and discussion

3.1. 3D multi-aspect shape characteristics

Based on the already reconstructed surface morphology of total 224 lunar regolith particles aided with the X-ray μCT scanning and

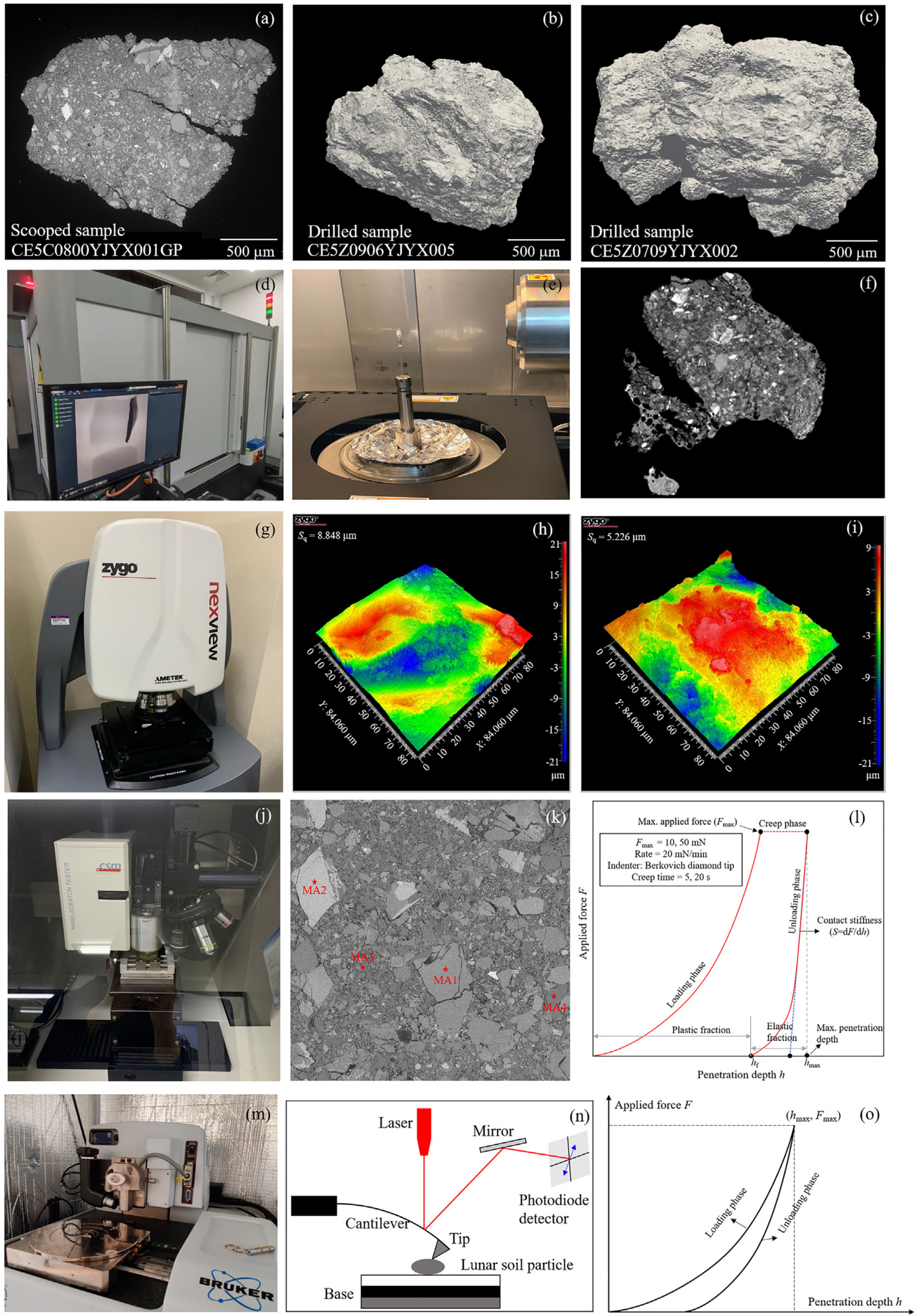

Fig. 1. Chang'e-5 lunar samples and microscopic test apparatus accompanied with the corresponding schematic diagrams. (a) Scooped sample CE5C0800YJYX001GP; (b) drilled sample CE5Z0906YJYX005; (c) drilled sample CE5Z0709YJYX002; (d) HeliScan X-ray μCT scanning apparatus; (e) interior view of X-ray μCT scanning apparatus; (f) slice of raw μCT image; (g) ZYGO NexView 3D white light interferometry apparatus; (h) 3D flattened surface roughness profile of CE5Z0709YJYX002 with 84 μm × 84 μm field of view (S_q: particle surface roughness); (i) 3D flattened surface roughness profile of CE5Z0906YJYX005 with 84 μm × 84 μm field of view; (j) Hysitron TI 980 TriboIndenter (Bruker) nanoindentation apparatus; (k) four chosen measurement areas (i.e., MA1–MA4) within the CE5C0800YJYX001GP for the nanoindentation test; (l) illustrative applied force F-penetration depth h curve for the nanoindentation test using nanoindentor (F_{max}: maximum applied force; h_{max}: maximum penetration depth; h_f: unloading residual depth; S: contact stiffness); (m) Bruker (Icon) AFM apparatus; (n) schematic representation of the AFM operation; (o) illustrative applied force F-penetration depth h curve for the nanoindentation test using AFM.

image processing techniques, their aspect ratio *AR*, sphericity *S*, convexity *C* and roundness *R* were determined according to the previous literature (e.g., [27–29]). The specific definitions of these shape indices can be referenced to Fig. S1 (online). Fig. 2 gives the cumulative distribution function curves of these shape parameters accompanied with the corresponding ones for 106 Leighton Buzzard sand (LBS) particles and 78 highly decomposed granite (HDG) particles published in the previous literature (e.g., [30,31]). LBS is a typical hydraulically transported soil exploited from the town of Leighton Buzzard in southeast England while HDG is a representative granite residual soil widely distributed in Hong Kong. Both two types of soils can capture the particle shape variation of terrestrial soils to some extent. It can be seen from Fig. 2 that the average values of *AR*, *S*, *C*, and *R* of Chang'e-5 lunar samples are obviously smaller than those of HDG and LBS particles, suggesting that lunar regolith particles are more irregular and angular than terrestrial soil particles. Meanwhile, Table S1 (online) presents the particle average roughness values of BYX002 and BYX005 evaluated with different sized fields of view, which shows that the particle surface roughness depends on the actual size of field of view and generally increases with the view size. In order to reasonably compare the surface topological feature of lunar regolith particles with that of terrestrial geomaterial particles, Table S1 (online) summarizes the particle surface roughness of common terrestrial geomaterial particles at similar sized fields of view (i.e., 20 μm × 20 μm or 30 μm × 30 μm). It presents that the BYX002 exhibits larger particle surface roughness (i.e., 1.75 μm) than most of terrestrial geomaterials including the CDG particles (i.e., 1.34 μm, after Ref. [32]) and DNA-1A lunar soil simulant (i.e., 1.48 μm, after Ref. [33]), except for the pumice particles (i.e., 2.39 μm, after Ref. [34]) and MMS-1 Martian soil simulant particles (i.e., 2.09 μm, after Ref. [35]), while the BYX005 owns the largest surface roughness (i.e., 3.11 μm).

The essential reason accounting for distinct 3D multi-aspect shape characteristics for lunar regolith and terrestrial geomaterial particles is their distinct formation and evolution mechanisms, which further reflects dissimilar Earth and Moon surface processes. Specifically, terrestrial soil particles are generally created from rocks through a series of Earth weathering processes related with the water, air and biology, and then may experience the long-term transportation and depositing processes dominated by the water or wind, during which the particles would be smoothed and polished for transported soils (e.g., LBS). While for lunar regolith particles, they are primarily generated by the everlasting impacts of micrometeorites/meteorites, which has given it a final average *AR* of 0.751, more close to the 2D silver ratio (0.707) that represents the *AR* value of fragments produced by hypervelocity impact experiments (e.g., [36,37]). The slight deviation herein may be due to the mechanical abrasion of lunar regolith particles during the impact gardening, resulting in a slightly larger average

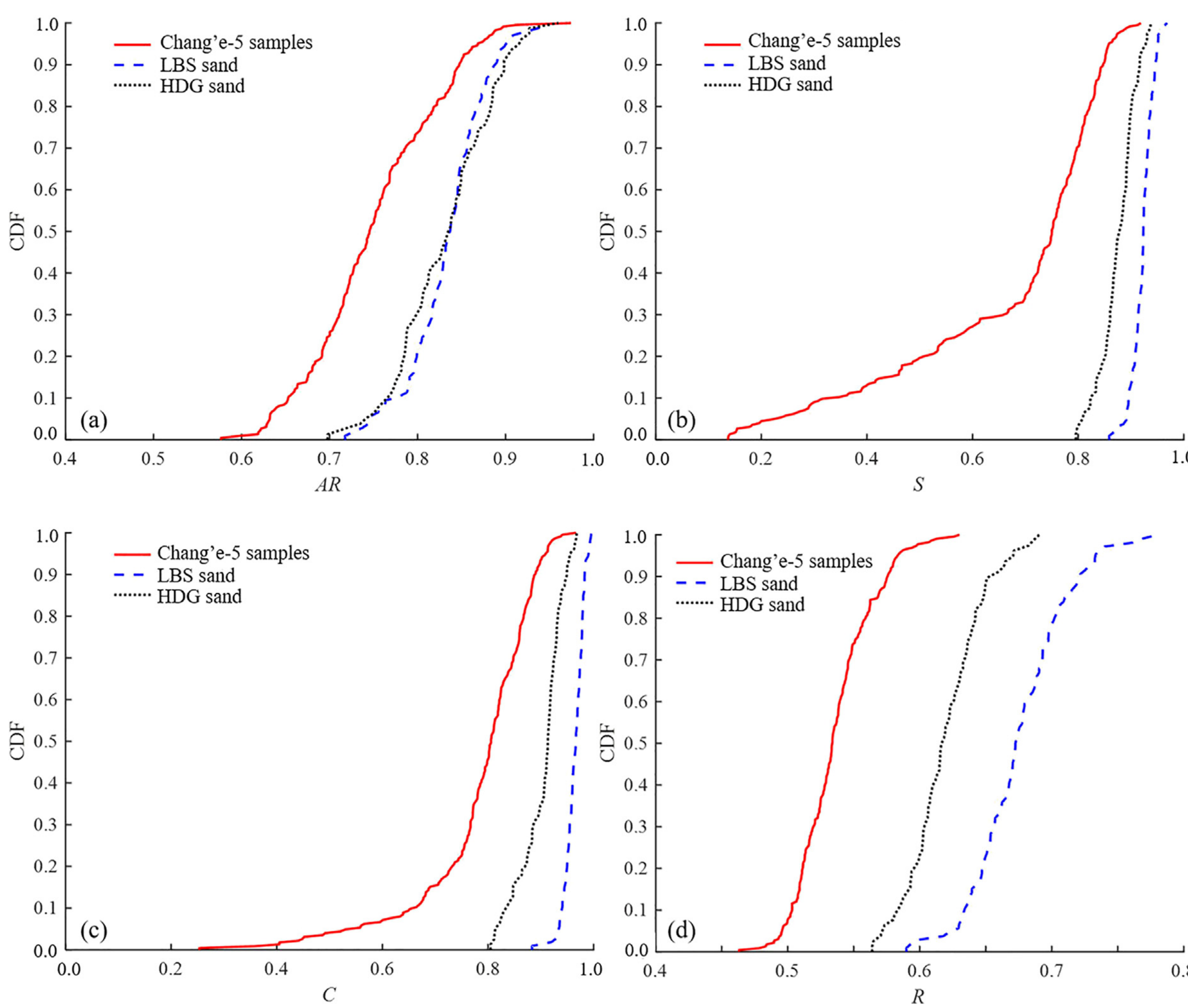

Fig. 2. Cumulative distribution functions (CDFs) of particle shape indices of Chang'e-5 lunar samples and two representative terrestrial soil particles (LBS: Leighton Buzzard sand; HDG: highly decomposed granite) in terms of global form and local roundness aspects. (a) Aspect ratio *AR*; (b) sphericity *S*; (c) convexity *C*; (d) roundness *R*.

value of *AR* than that of hypervelocity impact fragments, but still smaller than those of LBS and HDG particles. In addition, the constant space weathering has altered surface microstructures of lunar regolith particles especially at the micro- or nano-scales, thus giving them larger surface roughness compared with the DNA-1A lunar soil simulant. This observation suggests that the particle roughness needs to be taken as an additional index for evaluating the fidelity of lunar soil simulants although their particle shape characteristics can be similar with those of real lunar regolith at large scales through mechanical crushing and abrasion.

3.2. Young's modulus and hardness

Fig. 3 gives nanoindentation test curves of four MAs in BYX001GP under different combinations of maximum applied force F_{max} and creep time t_c, while Fig. 4 presents the statistics of relevant physical quantities. From Fig. 4a, we can see that given F_{max} and t_c, MA3 shows the greatest mean maximum penetration depth h_{max} while MA1 exhibits the smallest one, which indicates that the reduced modulus and hardness of MA1 and MA3 are the largest and smallest values, respectively, among four MAs, as shown in Fig. 4e, f. MA2 has the second largest reduced modulus and hardness followed by MA4. Note that the indentation stiffness of four MAs does not strictly follow the same pattern with the reduced modulus and hardness due to the contact area effect. For instance, Fig. 4d illustrates that MA3 has a slightly larger indentation stiffness than MA4 because of the greater penetration depth and hence the larger contact area. In addition, the creep displacements in Fig. 4c for four MAs follow the similar pattern as the maximum penetration depth, indicating that the lunar sample surface material with less Young's modulus or hardness is more likely to expand under the indenter when subjected to unloading. Fig. 4b, d presents that the variation of indentation stiffness and elastic fraction of four MAs follows an opposite trend, that is, the indented area with a larger indentation stiffness has a smaller elastic fraction.

The distinct mechanical properties illustrated by varying nanoindentation curves in Fig. 3 for four MAs at the same F_{max} and t_c mainly result from their different mineral compositions and microstructural features. With the aid of scanning electron microscopy (SEM) equipped with the energy-dispersive X-ray spectroscopy (EDS), the elemental compositions and surface fabrics of four MAs are determined, and analysis results are presented in Figs. S2 and S3 (online), respectively. It can be seen from Fig. S2 (online) that elemental compositions are distinct for four MAs, and MA1, MA2, and MA4 are predicted as olivine, ilmenite, and pyroxene, respectively, according to the weight percentages of elements. The relative sizes of hardness values for three predicted mineral phases are basically consistent with those of measured average values herein (Fig. 4f). For MA3, Fig. S3 (online) shows that it has

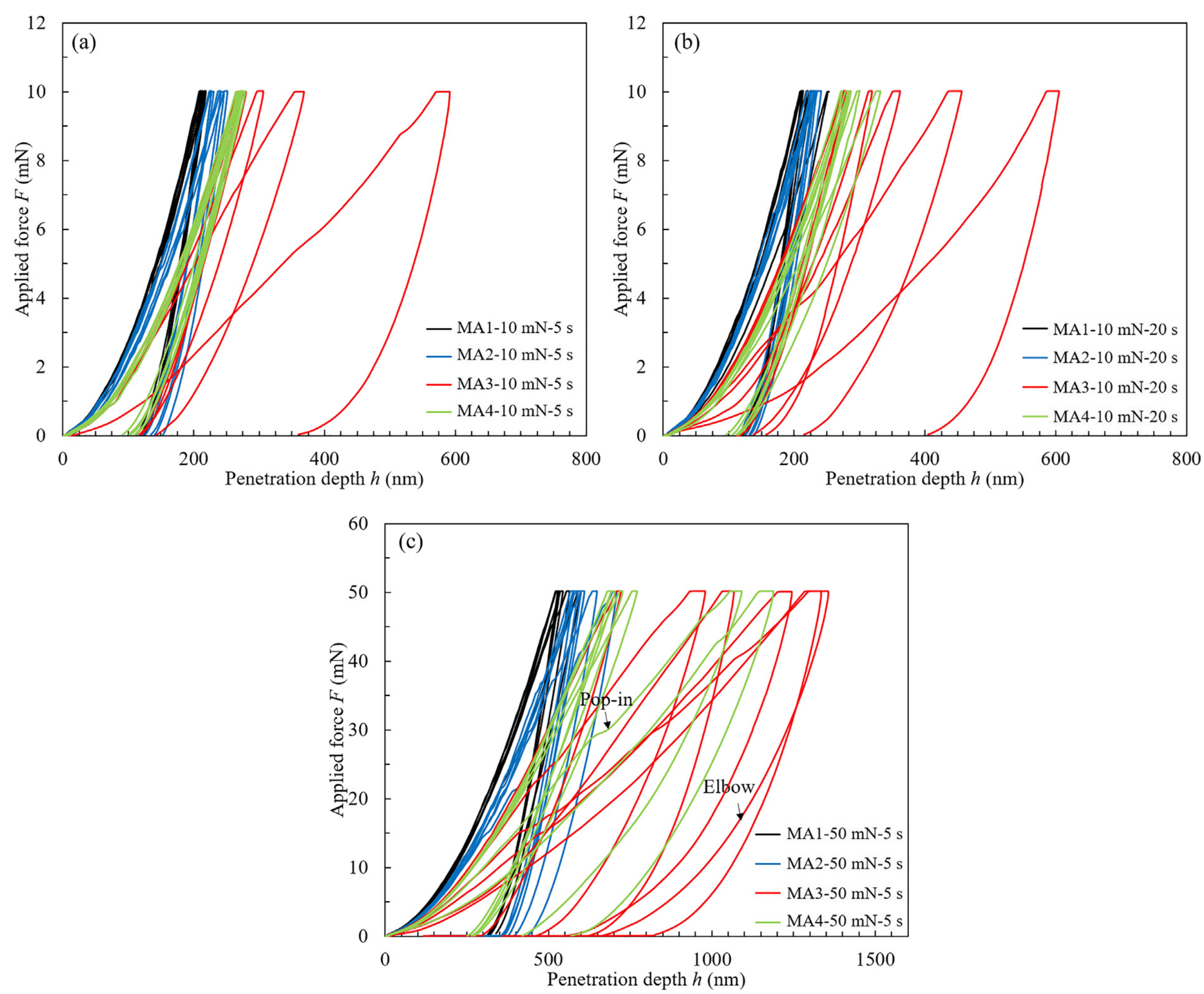

Fig. 3. Nanoindentation applied force *F*-penetration depth *h* curves of four different measurement areas (i.e., MA1–MA4) for BYX001GP under different combinations of maximum applied force F_{max} and creep time t_c. (a) F_{max} = 10 mN and t_c = 5 s; (b) F_{max} = 10 mN and t_c = 20 s; (c) F_{max} = 50 mN and t_c = 5 s.

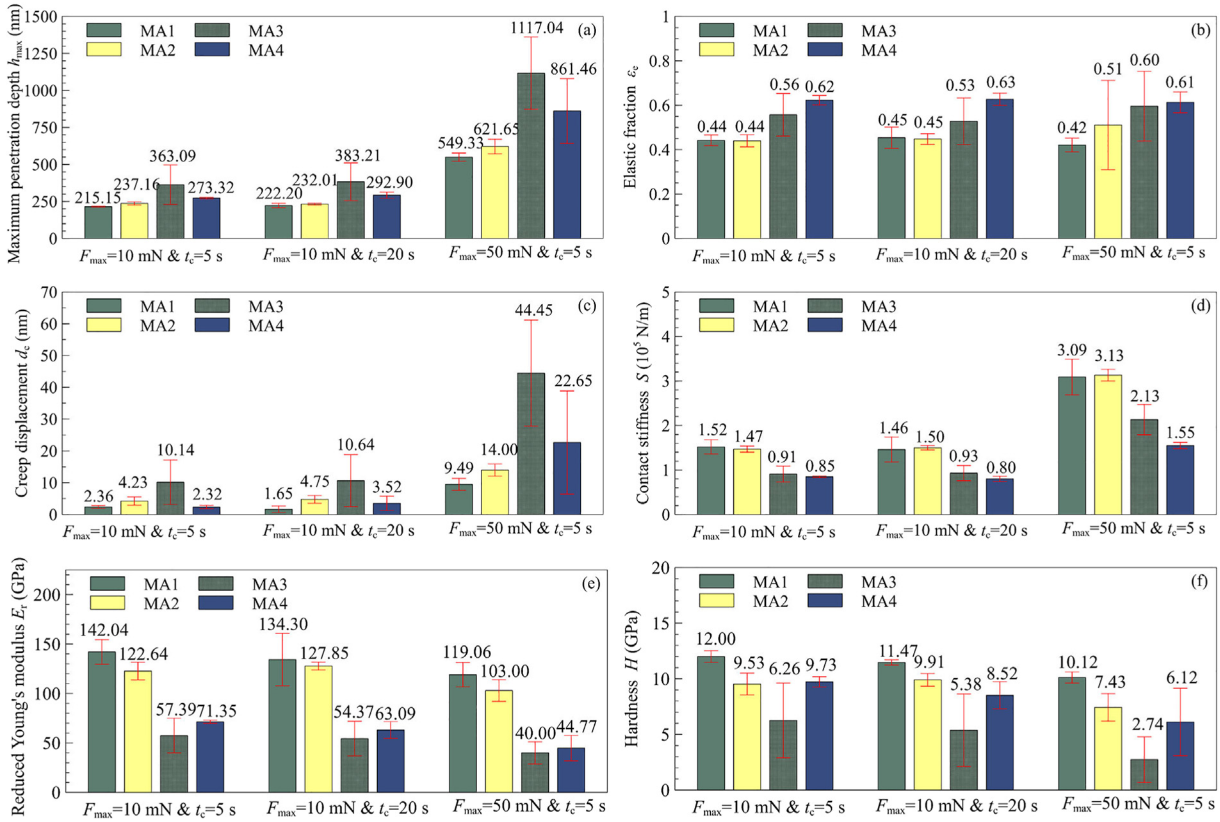

Fig. 4. Statistics of relevant physical quantities of four different measurement areas (i.e., MA1–MA4) for BYX001GP derived from nanoindentation tests under different combinations of F_{max} and t_c. (a) Maximum penetration depth h_{max}; (b) elastic fraction ε_e; (c) creep displacement d_c; (d) indentation contact stiffness S; (e) reduced Young's modulus E_r; (f) hardness H. The standard deviation of each data set is shown on the respective column as error bar, and the corresponding mean value is labeled at the top of each column.

a visibly discontinuous surface matrix with relatively larger pore structures compared with highly dense and compacted fabrics of other three MAs. This surface microstructure difference has led MA3 own a smaller average hardness or average reduced modulus and larger variability of mechanical properties, which is highlighted by the more significant dispersion of nanoindentation curves for MA3 in Fig. 3. The relatively pure mineral compositions and compacted surface fabrics of MA1, MA2, and MA4 have made nanoindentation curves of different indented spots within these MAs basically collapsed with each other, in spite of with a certain variability due to the inherent heterogeneity of lunar sample materials. One exception for MA4 under F_{max} = 50 mN and t_c = 5 s in Fig. 3c is mainly ascribed to two special indentation spots (i.e., red triangle marks in Fig. S3d online) that locate at or near the pores between different mineral phases. In addition, typical "pop-in" and "elbow" events have been observed from nanoindentation curves (e.g., Fig. 3c), which are mainly caused by the creation of micro-cracking (red circle marks in Fig. S3 online) or encountered in the pores or micro-defects (red triangle marks in Fig. S3 online) and material expansion due to the phase transformation, respectively.

Furthermore, from Fig. 4, we can see that the creep time t_c has a negligible influence on mechanical properties of BYX001GP within the studied range, while with the increase of the maximum applied force F_{max}, the pressure-related maximum penetration depth h_{max}, creep displacement d_c and indentation stiffness S increase. Considering that the F_{max} and t_c have relatively limited influences on the reduced Young's modulus and hardness, the Young's modulus and hardness of four MAs under all cases are averaged as the final particle Young's modulus (i.e., 81.89 GPa) and hardness (i.e., 8.27 GPa) of BYX001GP, respectively. Interestingly, the particle hardness and Young's modulus of BYX001GP are strikingly comparable with those of particles returned from the surface of the asteroid 25143 Itokawa (i.e., with the Young's modulus of 76.44–94.66 GPa and hardness of 8.50–12.00 GPa, see Table S1 online) [38], which are mainly attributed to their similar mineral compositions (e.g., olivine and pyroxene) for both extra-terrestrial soil particles.

For nanoindentation results of BYX002 and BYX005 with the AFM, Fig. 5a, b presents the corresponding test curves under two different F_{max}, while Fig. 5c summarizes the corresponding statistics of Young's modulus derived from these curves. It can be seen that at the given F_{max} the Young's modulus of each lunar basalt particle exhibits very large variabilities for different indented spots, while the average value changes insignificantly under two loading cases. Hence, the Young's modulus values of all cases are averaged as the particle Young's modulus of two lunar basalt clasts. The Young's modulus values of BYX002 and BYX005 are determined as 24.64 and 4.49 GPa, respectively, as summarized in Table S1 (online). We have noticed that both two lunar basalt clasts exhibit totally distinct Young's modulus and particle surface roughness, which may because they have experienced different lunar surface exposure times and meteorite collision processes. According to the previous analysis on basic stratigraphy of the shallow regolith at Chang'e-5 sampling site and the possible ejecta source [39,40], and also the relationship between the drilling displacement and sample dissected position in the soft tube estimated by sample IDs [26], both two lunar basalt clasts were sampled in different depths, and the ejecta including top lunar basalt clast BYX002 might undergo more meteorite impacts and space weathering, which had changed its surface microstructure

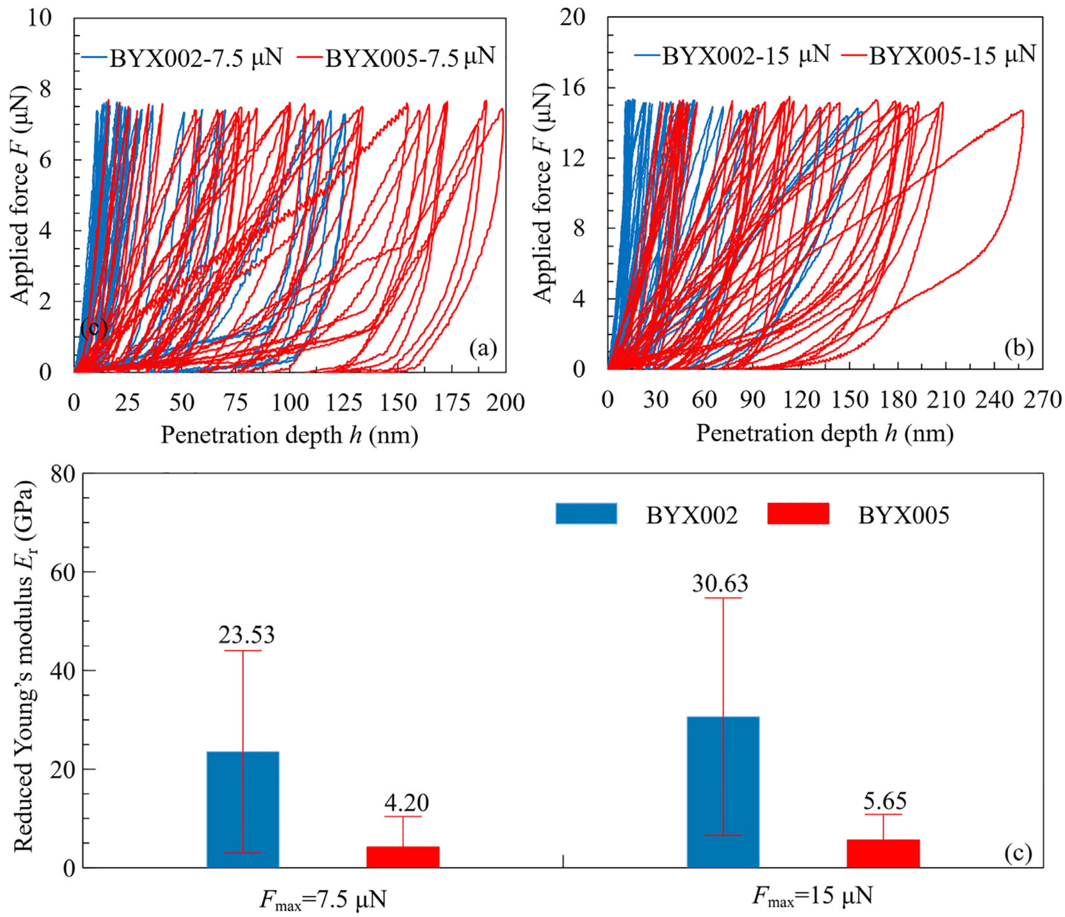

Fig. 5. Nanoindentation results for two lunar basalt clasts using the AFM. (a) Applied force *F*-penetration depth *h* curves for BYX002 and BYX005 under F_{max} = 7.5 μN; (b) applied force *F*-penetration depth *h* curves for BYX002 and BYX005 under F_{max} = 15 μN; (c) statistics of reduced modulus of BYX002 and BYX005.

and mineral compositions, thus exhibiting distinct tribological and mechanical properties with the bottom lunar basalt clast BYX005. This observation suggests that it may be possible to understand the shallow stratigraphic information of Chang'e-5 sampling site by comparing particle property differences of drilled samples at different depths for future lunar sample studies.

3.3. Predicted interparticle friction coefficient

The interparticle friction coefficient μ_p is an important property to characterize the influence of particle roughness on sliding resistance between granular particles, and can be directly measured by micromechanical slip tests for terrestrial geomaterials. This approach is currently not applicable for valuable lunar regolith samples due to the possible damage or contamination. Herein we adopt an indirect experimental fitting method to predict μ_p values of lunar regolith particles. Fig. 6a–c presents correlations between μ_p and particle roughness S_q, particle Young's modulus E_p, and hardness H_p based on the already published experimental data on more than ten different types of terrestrial geomaterials or engineering materials [32–35,42–44] (summarized in Table S1 online). It can be obviously seen that μ_p relates to these three quantities significantly. Among which, μ_p increases with S_q while decreases with E_p and H_p with different power functions, and the variation trend of μ_p with S_q is also consistent with that presented in Ref. [41], where influence of particle roughness on the interface friction coefficient was solely investigated through glass specimens with different roughness. Considering that H_p also has a power law relationship with E_p, as shown in Fig. 6d, and in order to avoid the more complex and redundant fitting relating μ_p with S_q, E_p, and H_p together based on the limited experimental data, a relatively simple and robust spatial fitting between μ_p and S_q and E_p has been constructed in Fig. 6e to predict μ_p values of two lunar basalt clasts (i.e., 0.48 for BYX002 and 0.76 for BYX005, summarized in Table S1 online). The predicted μ_p values of the lunar regolith particles are basically larger than most of terrestrial geomaterials and engineering materials, except for the pumice and MMS-1 particles.

3.4. Prediction of residual friction angle of lunar regolith

Due to the limited amount of lunar samples currently available for geotechnical engineers, it is not very practical to conduct geomechanical experiments to acquire engineering properties of the lunar regolith, which are key to the future lunar base establishment and resource utilization. Herein, we attempt to predict the residual friction angle φ_c of lunar regolith from the already determined geometrical and tribological properties of Chang'e-5 lunar samples. Many experimental or numerical studies have shown that the particle shape and interparticle friction play more significant roles in the residual friction angle of granular soils than the particle grading (e.g., [45–48]), although the studied particle grading range is still relatively narrow compared with that of lunar regolith. In addition, Modenese [49] had pointed out that very little cohesion was recorded for lunar regolith at the residual state, and the surface energy force hardly affected the residual friction angle of lunar regolith. Hence, according to our previous discrete element mod-

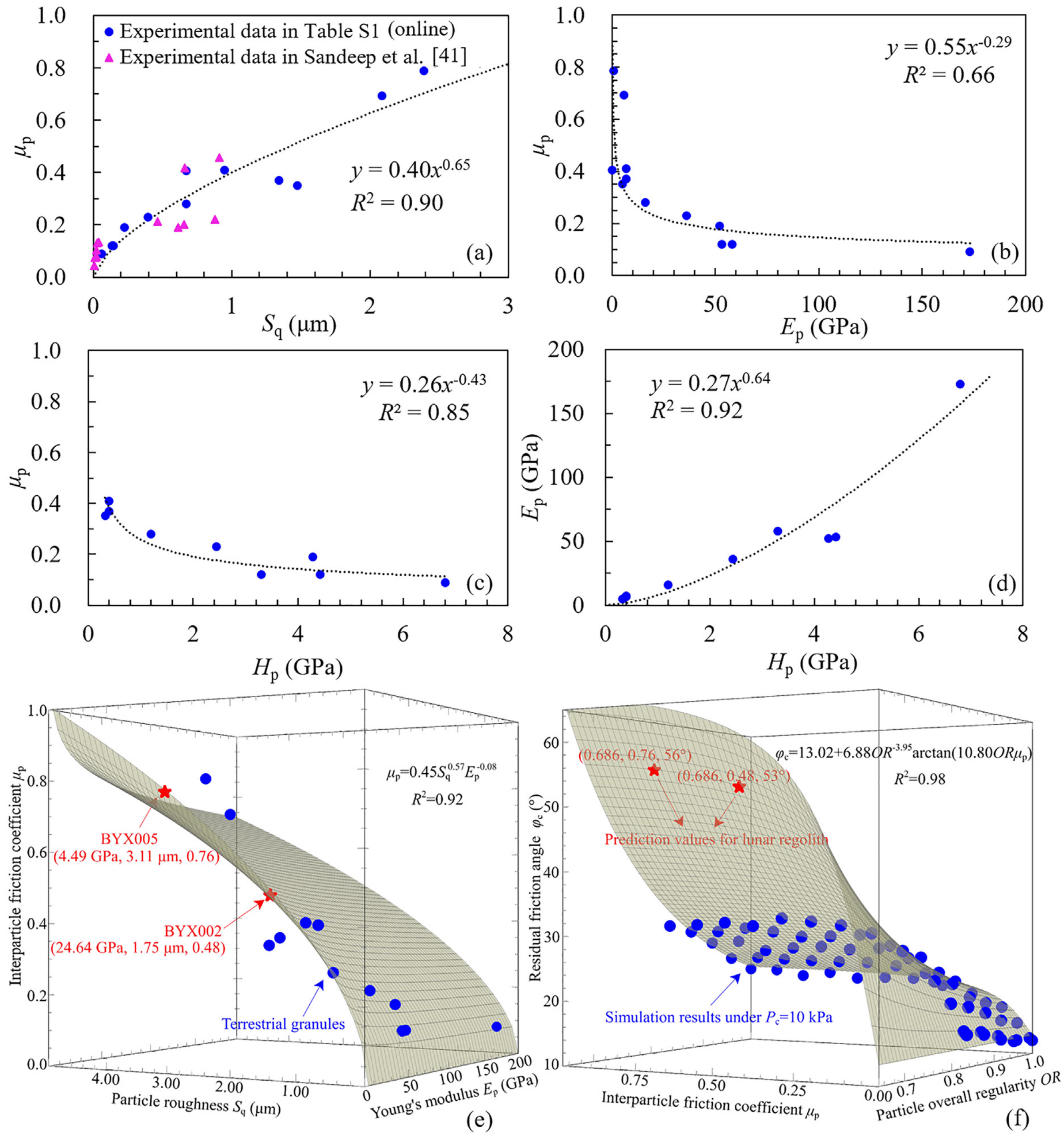

Fig. 6. Prediction of interparticle friction coefficient μ_p for lunar basalt clasts and residual friction angle φ_c for lunar regolith. Correlations between μ_p and particle roughness S_q (a) [41], particle Young's modulus E_p (b), and particle hardness H_p (c); (d) correlation between H_p and E_p; (e) predicted μ_p of two lunar basalt clasts BYX002 and BYX005 according to the spatial fitting plane based on S_q and E_p; (f) predicted φ_c of lunar regolith based on particle overall regularity (*OR*) and μ_p. Blue circle points represent our discrete element method (DEM) triaxial shearing test results of uniformly graded sands with different combinations of *OR* and μ_p under the low confining pressure of 10 kPa.

elling considering realistic particle shape [29,47], a series of triaxial shearing tests on uniformly graded samples of different particle overall regularity (*OR*) (0.835, 0.876, 0.918, 0.958, and 1.000) and μ_p (0.001, 0.01, 0.05, and 0.10–1.00 with an interval of 0.10) have been conducted under low confining pressure (i.e., 10 kPa) to acquire the corresponding φ_c values considering of the low gravity level on the Moon. Based on these numerical results (blue sphere points in Fig. 6f), φ_c of lunar regolith is predicted in the range of 53° to 56° (red star points in Fig. 6f) through the data fitting method. Herein the OR is defined as the mean value of average *AR*, *S*, *C*, and *R* of Chang'e-5 lunar samples and is determined as 0.686 from previous 3D multi-aspect shape indices. The predicted μ_p of 0.48 for BYX002 and 0.76 for BYX005 are adopted as upper and lower bounds to estimate the range of φ_c considering of the uncertainty when predicting the representative μ_p of lunar regolith particles from currently limited particle property data. It is interesting to see that the range of φ_c for the lunar regolith simulant DNA-1A (e.g., 47°–56° in Ref. [50]) under similar low confining pressure is consistent with our predicted range. Note that microscopic tests presented in this study should be conducted on more lunar regolith particles in following studies to further reduce the prediction uncertainty. In addition, indoor tests on the lunar soil simulant with similar particle mechanical, geometrical and tribological properties as Chang'e-5 lunar samples need to be conducted to further improve the prediction of residual friction angle of lunar regolith by considering the possible effect of particle grading.

4. Conclusion

In this contribution, we for the first time quantified 3D multi-aspect shape characteristics, and mechanical and tribological properties of Chang'e-5 lunar samples using a series of non-destructive microscopic tests. Based on that, the residual friction angle of lunar regolith under low confining pressure was reasonably predicted. The presented results provide a new idea for cross-scale estimating engineering properties of lunar regolith under limited lunar samples. Some primary conclusions are summarized as follows.

(1) The average particle aspect ratio, sphericity, convexity, and roundness of lunar samples are apparently smaller in magnitude than those of typical hydraulically transported soil and igneous saprolitic rock, while their surface roughness values are obviously larger than those of most of terrestrial geomaterials or engineering materials including DNA-1A lunar regolith simulant. These 3D multi-aspect shape differences indicate that the lunar regolith particles are more irregular, angular and rough than most of terrestrial soil particles due to their unique formation and evolution processes.

(2) A simple relationship between the interparticle friction coefficient and particle Young's modulus and particle roughness has been well proposed to predict interparticle friction coefficients of lunar regolith particles to avoid the possible damage or contamination on valuable lunar samples when directly measuring this quantity using micromechanical slip tests.

(3) The residual friction angle of lunar regolith is predicted within the range of 53° to 56° according to the measured particle overall regularity and interparticle friction coefficient of Chang'e-5 lunar samples, and the residual friction angle of DNA-1A lunar regolith simulant is within the predicted range under the similar low confining pressure.

Conflict of interest

The authors declare that they have no conflict of interest.

Acknowledgments

This work was supported by the National Natural Science Foundation of China (42241109 and 42202297) and Tsinghua University Initiative Scientific Research Program (20211080097). We would like to appreciate the China National Space Administration (CNSA) for providing us with invaluable lunar samples from the Chang'e-5 mission. We also thank Drs. Hengci Tian and Chi Zhang at the Institute of Geology and Geophysics, Chinese Academy of Sciences, and Miss Yimai Liang, Ms. Wenyan Yang, Mr. Jianguo Jiao, Dr. Hao Zhan, and Mr. Junjie Xiong at the State Key Laboratory of Tribology, Tsinghua University for the arduous and cautious experimental works.

Author contributions

Jiayan Nie and Yifei Cui contributed to the conceptualization, experimental design, and funding acquisition of the whole work. Kostas Senetakis, Dan Guo, Yu Wang, Guodong Wang, Peng Feng, Huaiyu He, and Xuhang Zhang analyzed the data and interpreted the results. Jiayan Nie wrote the original manuscript. Yifei Cui, Xiaoping Zhang, Cunhui Li, Hu Zheng, Wei Hu, Fujun Niu, Quanxing Liu, and Anyuan Li reviewed and revised the manuscript. All authors discussed the results. Yifei Cui supervised the project.

Appendix A. Supplementary materials

Supplementary materials to this article can be found online at https://doi.org/10.1016/j.scib.2023.03.019.

References

[1] Scott RF, Carrier WD, Costes NC, et al. Apollo 12 soil mechanics investigation. Geotechnique 1971;21:1–14.
[2] Jaffe LD. Shear strength of lunar soil from Oceanus Procellarum. Moon 1973;8:58–72.
[3] Carrier III WD, Olhoeft GR, Mendell W. Physical properties of the lunar surface. In: Heiken GH, Vaniman DT, French BM, editors. Lunar sourcebook, a user's guide to the Moon. Cambridge: Cambridge University Press; 1991. p. 475–594.
[4] Slyuta EN. Physical and mechanical properties of the lunar soil (a review). Solar Syst Res 2014;48:330–53.
[5] Smith M, Craig D, Herrmann N, et al. The Artemis Program: an overview of NASA's activities to return humans to the moon. Proceedings of the 2020 IEEE Aerospace Conference. New York: IEEE; 2020.
[6] Zhou CY, Jia YZ, Liu JZ, et al. Scientific objectives and payloads of the lunar sample return mission-Chang'e-5. Adv Space Res 2022;69:823–36.
[7] Qian YQ, Xiao L, Wang Q, et al. China's Chang'e-5 landing site: geology, stratigraphy, and provenance of materials. Earth Planet Sci Lett 2021;561:116855.
[8] Che X, Nemchin A, Liu D, et al. Age and composition of young basalts on the moon, measured from samples returned by Chang'e-5. Science 2021;374:887–90.
[9] Hu S, He HC, Ji JL, et al. A dry lunar mantle reservoir for young mare basalts of Chang'e-5. Nature 2021;600:49–53.
[10] Li QL, Zhou Q, Liu Y, et al. Two-billion-year-old volcanism on the moon from Chang'e-5 basalts. Nature 2021;600:54–8.
[11] Li C, Hu H, Yang MF, et al. Characteristics of the lunar samples returned by the Chang'e-5 mission. Natl Sci Rev 2022;9:nwab188.
[12] Tian HC, Wang H, Chen Y, et al. Non-KREEP origin for Chang'e-5 basalts in the Procellarum KREEP TERRANE. Nature 2021;600:59–63.
[13] Zhang H, Zhang X, Zhang G, et al. Size, morphology, and composition of lunar samples returned by Chang'e-5 mission. Sci China Phys Mech Astron 2022;65:229511.
[14] Katagiri J, Matsushima T, Yamada Y, et al. Investigation of 3D grain shape characteristics of lunar soil retrieved in Apollo 16 using image-based discrete-element modeling. J Aerosp Eng 2015;28:04014092.
[15] Mitchell JK, Houston WN, Carrier W, et al. Apollo soil mechanics experiment S-200, final report. Washington DC: NASA; 1974.
[16] Antony S, Moreno-Atanasio R, Hassanpour A. Influence of contact stiffnesses on the micromechanical characteristics of dense particulate systems subjected to shearing. Appl Phys Lett 2006;89:214103.
[17] Barreto D, O'Sullivan C. The influence of inter-particle friction and the intermediate stress ratio on soil response under generalised stress conditions. Granul Matter 2012;14:505–21.
[18] Goncu F, Luding S. Effect of particle friction and polydispersity on the macroscopic stress-strain relations of granular materials. Acta Geotech 2013;8:629–43.
[19] Shaheen MY, Thornton AR, Luding S, et al. The influence of material and process parameters on powder spreading in additive manufacturing. Powder Technol 2021;383:564–83.
[20] Vangla P, Latha GM. Influence of particle size on the friction and interfacial shear strength of sands of similar morphology. Int J Geosynth Groun 2015;1:1–12.
[21] Yang J, Luo XD. Exploring the relationship between critical state and particle shape for granular materials. J Mech Phys Solids 2015;84:196–213.
[22] Chen XF, Carpenter BM, Reches Z. Asperity failure control of stick-slip along brittle faults. Pure Appl Geophys 2020;177:3225–42.
[23] Misra A. Effect of asperity damage on shear behavior of single fracture. Eng Fract Mech 2002;69:1997–2014.
[24] Misra A, Marangos O. Rock-joint micromechanics: relationship of roughness to closure and wave propagation. Int J Geomech 2011;11:431–9.
[25] Ahamed MAA, Perera MSA, Matthai SK, et al. Coal composition and structural variation with rank and its influence on the coal-moisture interactions under coal seam temperature conditions—a review article. J Petrol Sci Eng 2019;180:901–17.
[26] Zheng Y, Yang M, Deng X, et al. Analysis of Chang'e-5 lunar core drilling process. Chin J Aeronaut 2022;36:292–303.
[27] Barrett PJ. The shape of rock particles, a critical review. Sedimentology 1980;27:291–303.
[28] Zhao B, Wang J. 3D quantitative shape analysis on form, roundness, and compactness with μCT. Powder Technol 2016;291:262–75.
[29] Nie JY, Shi XS, Cui Y, et al. Numerical evaluation of particle shape effect on small strain properties of granular soils. Eng Geol 2022;303:106652.
[30] Wei D, Wang J, Nie JY, et al. Generation of realistic sand particles with fractal nature using an improved spherical harmonic analysis. Comput Geotech 2018;104:1–12.
[31] Nie JY, Li DQ, Cao ZJ, et al. Probabilistic characterization and simulation of realistic particle shape based on sphere harmonic representation and Nataf transformation. Powder Technol 2020;360:209–20.

[32] Sandeep CS, Senetakis K. Effect of young's modulus and surface roughness on the inter-particle friction of granular materials. Materials 2018;11:217.
[33] Sandeep CS, Marzulli V, Cafaro F, et al. Micromechanical behavior of DNA-1A lunar regolith simulant in comparison to Ottawa sand. J Geophys Res-Solid Earth 2019;124:8077–100.
[34] He H, Senetakis K. An experimental study on the micromechanical behavior of pumice. Acta Geotech 2019;14:1883–904.
[35] Kasyap SS, Senetakis K. A grain-scale study of Mojave Mars Simulant (MMS-1). Sensors 2021;21:4730.
[36] Capaccioni F, Cerroni P, Coradini M, et al. Shapes of asteroids compared with fragments from hypervelocity impact experiments. Nature 1984;308:832–4.
[37] Fujiwara A, Kamimoto G, Tsukamptp A. Expected shape distribution of asteroids obtained from laboratory impact experiments. Nature 1978;272:602–3.
[38] Tanbakouei S, Trigo-Rodríguez JM, Sort J, et al. Mechanical properties of particles from the surface of asteroid 25143 Itokawa. Astron Astrophys 2019;629:A119.
[39] Qian Y, Xiao L, Head JW, et al. Copernican-aged (< 200 Ma) impact ejecta at the Chang'e-5 landing site: statistical evidence from crater morphology, morphometry, and degradation models. Geophys Res Lett 2021;48. e2021GL095341.
[40] Su Y, Wang R, Deng X, et al. Hyperfine structure of regolith unveiled by Chang'e-5 lunar regolith penetrating radar. IEEE Trans Geosci Remote Sen 2022;60:5110414.
[41] Sandeep CS, Li S, Senetakis K. Scale and surface morphology effects on the micromechanical contact behavior of granular materials. Tribol Int 2021;159:106929.
[42] Ren J, He H, Lau K-C, et al. Influence of iron oxide coating on the tribological behavior of sand grain contacts. Acta Geotech 2022;17:2907–29.
[43] Sandeep CS, Todisco MC, Nardelli V, et al. A micromechanical experimental study of highly/completely decomposed tuff granules. Acta Geotech 2018;13:1355–67.
[44] Ren J, Li S, He H, et al. The tribological behavior of iron tailing sand grain contacts in dry, water and biopolymer immersed states. Granul Matter 2021;23:1–23.
[45] Estrada N. Effects of grain size distribution on the packing fraction and shear strength of frictionless disk packings. Phys Rev E 2016;94:062903.
[46] Yang J, Luo XD. The critical state friction angle of granular materials: does it depend on grading? Acta Geotech 2018;13:535–47.
[47] Nie JY, Zhao S, Cui Y, et al. Coupled effects of particle overall regularity and sliding friction on the shear behavior of uniformly graded dense sands. J Rock Mech Geotech 2022;14:873–85.
[48] Nie JY, Zhao J, Cui Y, et al. Correlation between grain shape and critical state characteristics of uniformly graded sands: a 3D DEM study. Acta Geotech 2022;17:2783–98.
[49] Modenese C. Numerical study of the mechanical properties of lunar soil by the discrete element method Doctor Dissertation. Oxford: Oxford University; 2013.
[50] Marzulli V, Cafaro F. Geotechnical properties of uncompacted DNA-1A lunar simulant. J Aerosp Eng 2019;32:04018153.

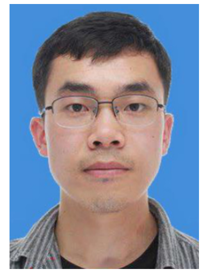

Jiayan Nie is currently an associate research fellow at Wuhan University and formerly a postdoctoral research fellow at Tsinghua University. He received his bachelor's and Ph.D. degrees from Shandong University and Wuhan University, respectively. His research focuses on exploring the salient static, transient, and flow behaviors of granular materials by means of the theoretical model, physical test, discrete element method, and hierarchical multi-scale model.

Yifei Cui is currently an associate professor at Tsinghua University, China. He received his bachelor's degree at the Hong Kong Polytechnic University, China and M.Sc. and Ph.D. degrees at University of Alberta, Canada. After graduation, he, as post-doctoral research fellow and research assistant professor in succession, worked at the Hong Kong University of Science and Technology, China. His research focuses on mechanical behaviors of granular materials using physical and numerical modellings.